Atmos. Meas. Tech. Discuss., 7, 7175–7206, 2014
www.atmos-meas-tech-discuss.net/7/7175/2014/
doi:10.5194/amtd-7-7175-2014

Atmospheric Measurement Techniques Discussions

Meso-scale modeling and radiative transfer simulations of a snowfall event over France at microwaves for passive and active modes and evaluation with satellite observations

V. S. Galligani[1], C. Prigent[1], E. Defer[1], C. Jimenez[3], P. Eriksson[2], J.-P. Pinty[4], and J.-P. Chaboureau[4]

[1]Laboratoire d'Etudes du Rayonnement et de la Matière en Astrophysique, CNRS, Observatoire de Paris, Paris, France
[2]Department of Earth and Space Sciences, Chalmers University of Technology, Gothenburg, Sweden
[3]Estellus, Paris, France
[4]Laboratoire d'Aérologie, UPS/CNRS, Toulouse, France

Received: 30 April 2014 – Accepted: 24 June 2014 – Published: 16 July 2014

Correspondence to: V. S. Galligani (victoria.galligani@obspm.fr)

Published by Copernicus Publications on behalf of the European Geosciences Union.

Abstract

Microwave passive and active radiative transfer simulations are performed with the Atmospheric Radiative Transfer Simulator (ARTS) for a mid-latitude snowfall event, using outputs from the Meso-NH mesoscale cloud model. The results are compared to the corresponding microwave observations available from MHS and CloudSat. The spatial structures of the simulated and observed brightness temperatures show an overall agreement since the large-scale dynamical structure of the cloud system is reasonably well captured by Meso-NH. However, with the initial assumptions on the single scattering properties of snow, there is an obvious underestimation of the strong scattering observed in regions with large frozen hydrometeor quantities. A sensitivity analysis of both active and passive simulations to the microphysical parameterizations is conducted. Simultaneous analysis of passive and active calculations provides strong constraints on the assumptions made to simulate the observations. Good agreements are obtained with both MHS and CloudSat observations when the single scattering properties are calculated using the "soft sphere" parameterization from Liu (2004), along with the Meso-NH outputs. This is an important step toward building a robust dataset of simulated measurements to train a statistically-based retrieval scheme.

1 Introduction

The quantification of the cloud and precipitating frozen phase at a global scale is important to monitor the full Earth energy budget and the hydrological cycle. However, the estimation of the frozen phase (ice and snow) from the present suite of satellite observations is still at a very early stage and remains an important challenge for future satellite instruments. As summarized in Noh et al. (2006), there are two major reasons for this. Firstly, the radiative signatures from falling snow are indistinguishable from liquid water signatures at visible and infrared wavelengths, and they are weak at low microwave frequencies (< 90 GHz). At higher microwave frequencies, snowfall

AMTD
7, 7175–7206, 2014

characterization from space is a challenging task, but possible through the analysis of the scattering signal from frozen hydrometeors (e.g. Katsumata et al., 2000; Bennartz and Bauer, 2003; Skofronick-Jackson and Johnson, 2011). The second, and main reason, is the complex nature and high variability of the microphysical properties (size, composition, density, and shape), and thus radiative properties, of the frozen particles (Johnson et al., 2012). The sensitivity to scattering depends on a large degree on the size and phase of the hydrometeors. In fact, there is a pressing need to constrain such microphysical properties from remote sensing in order to reduce the large uncertainties associated to ice contents in Numerical Weather Prediction and climate models (Waliser et al., 2009; Eliasson et al., 2011). Furthermore, an understanding of the bulk properties of frozen hydrometeors is essential to prepare for the next generation of microwave to sub-millimeter observations, i.e., the upcoming ESA MetOp-SG satellites with sub-mm frequency channels. Robust methods have to be developed to retrieve ice/snow parameters from satellite measurements. These methods are often based on large data sets of simulated observations. The accuracy of the retrieval largely depends on the quality of the simulated database and its representativity. As a first step in the development of such simulated database, this paper analyzes the sensitivity of simulated passive and active microwave observations to the microphysical properties of the frozen phase. The objective is to assess our capacity to simulate passive and active microwave observations in a consistent way, for snowfall situations. A meso-scale cloud model (Meso-NH) is coupled with a radiative transfer model (the Atmospheric Radiative Transfer Simulator, ARTS) and run for a real snowfall case. The results are compared with coincident satellite observations. The mesoscale cloud model outputs describe the atmospheric state of the scene at several time steps, including the relevant parameters necessary to conduct radiative transfer simulations of both passive and active real observations. The derived brightness temperatures (TBs) and equivalent radar reflectivities (Z_e) are compared to the available microwave observations from the Microwave Humidity Sounder (MHS) and the Cloud Profiling Radar (CPR).

AMTD
7, 7175–7206, 2014

This study is structured as follows. Section 2 presents one of the studied snowfall cases, and includes a description of Meso-NH model outputs and the coincident satellite observations. Section 3 briefly describes ARTS, along with the recently incorporated radar simulator module and a description of the microphysical properties to be analyzed. The sensitivity study of consistent active and passive radiative transfer simulations on such hydrometeor characteristics is presented in Sect. 4. Finally Sect. 5 draws conclusions.

2 A heavy snowfall event over France: Meso-NH simulations and microwave satellite observations

2.1 The meso-scale cloud model: Meso-NH

The non-hydrostatic mesoscale cloud model Meso-NH (Lafore et al., 1998), jointly developed by Météo-France and the Centre National de la Recherche Scientifique (CNRS), is a research model used in this study to simulate the atmospheric state of a heavy snowfall case over France. Meso-NH performance has been assessed in the past using space-borne sensors at various wavelengths (Chaboureau et al., 2000; Chaboureau et al., 2008; Wiedner et al., 2004; Meirold-Mautner et al., 2007) showing that neither strong nor systematic deficiencies are present in the microphysical scheme and in the prediction of the precipitating hydrometeor contents.

The Meso-NH microphysical scheme developed by Pinty and Jabouille (1998) predicts the evolution of the mixing ratios (mass of water per mass of dry air) of five hydrometeor categories: cloud droplets, rain drops, pristine ice crystals, snowflakes, and graupels. Meso-NH outputs include a full description of the atmospheric parameters (pressure, temperature, and mixing ratios for the water vapor, and the five hydrometer categories). The multiple interactions operating between the different water species are accounted for through the parameterization of 35 microphysical processes including nucleation, vapor/condensate exchanges, conversion, riming and sedimentation.

AMTD
7, 7175–7206, 2014

Together with the mixing ratios for each hydrometer category, the intrinsic microphysical scheme to Meso-NH describes some microphysical properties for each particle type at each layer of the atmosphere. This includes parameters such as the particle size distribution (PSD), the intrinsic mass, and the maximum particle diameter.

The concentration of the PSD is parametrized with a total number concentration N given by $N_h = C\lambda_h^x$, where the subscript h denotes the hydrometeor category, C and x are empirical constants derived from ground and in-situ measurements, and λ_h is known as the slope parameter of the size distribution. The size distribution of the hydrometeors is assumed to follow the generalized Gamma distribution,

$$n(D)\mathrm{d}D = N_h g(D)\mathrm{d}D = N_h \frac{\alpha}{\Gamma(\nu)} \lambda_h^{\alpha\nu} D^{\alpha\nu-1} \exp\left(-(\lambda_h D)^\alpha\right)\mathrm{d}D, \quad (1)$$

where D is the maximum dimension of complex shaped particles or the diameter for spherical particles, and $g(D)$ is the normalized distribution, which for $\alpha = \nu = 1$ reduces to the Marshall Palmer law.

Simple power laws describe the mass-size and the velocity-size relationships,

$$m = aD^b \quad (2)$$

$$v = cD^d \quad (3)$$

These relationships are taken to perform useful analytical integrations using the moment formula,

$$M(p) = \frac{G(p)}{\lambda_h^p} = \frac{1}{\lambda_h^p} \frac{\Gamma(\nu + p/\alpha)}{\Gamma(\nu)}, \quad (4)$$

AMTD
7, 7175–7206, 2014

where $M(p)$ is the pth moment of $g(D)$. Equation (4) can be used to compute the different hydrometeor mixing ratios q_h according to:

$$\rho_h q_h = \int_0^\infty m(D)n(D)\mathrm{d}D = aN_h M_h(b), \quad (5)$$

where ρ_h is the density of dry air. Table 1 describes the constants that characterize each of the hydrometeor species in the mentioned relations.

2.2 The case study

The selected scene corresponds to a strong snowfall event over France, 8 December 2010, very early in the cold season. This meteorological event led to huge disruptions of the transportation network over a large part of France, especially in the areas of Paris.

Meso-NH was initialized using ECMWF analyses available 8 December 2010 at 00:00 UTC and the lateral boundaries are linearly interpolated from ECMWF 6-hourly analyses (successively taken at 06:00 UTC, 12:00 UTC, etc.). The simulation domain contains 192 × 192 grid points at 20 km resolution, centered approximately in Paris. A second model at 5 km resolution with 256 × 256 grid points is gridnested and centered at the same place. Both domains contain a vertical grid with 48 levels unevenly spaced, with layer thickness varying from 50 m close to the surface and up to 1000 m at the top of the atmosphere.

Meso-NH model outputs are available every hour for this scene and the outputs at 13:00 UTC, corresponding to the over-pass of satellites onboard the A-train mission and NOAA-18, are analyzed in this study. Figure 1 presents the total columns of water vapor, cloud, rain, graupel, snow, and ice, as simulated by Meso-NH at 13:00 UTC.

AMTD
7, 7175–7206, 2014

2.3 Coincident satellite observations

This study focuses on high frequency microwave radiative transfer simulations and their evaluation with coincident passive and active observations. As mentioned earlier, the A-train mission and NOAA-18 over-passed the region modeled by Meso-NH at approximately 13:00 UTC. The satellite instruments of interest here are MHS (Bonsignori, 2007) onboard NOAA-18 and the CPR radar (Stephens et al., 2002) onboard CloudSat, a satellite on the A-train constellation.

MHS is a cross-track humidity sounder with surface zenith angles varying between 0° and 58°. The channels are located at 89.0, 157.0, 183.3 ± 1, 183.3 ± 3 and 190.3 GHz. The channels near the water vapour line of 183.3 GHz are opaque because of atmospheric absorption, in contrast to the more transparent window channels at 89, 157 and 190 GHz. The spatial resolution at nadir is 16 km for all channels and increases away from nadir (26 km at the furthest zenith angle along track). The polarization state is variable and results from a combination of the two orthogonal linear polarizations (V and H), with the polarization mixing depending on the scanning angle. The CPR onboard CloudSat is a 94 GHz nadir-looking radar that measures the power backscattered by cloud and precipitating particles as a function of distance from the radar. It has a footprint of 1.4 km (cross-track) and 1.7 km (along-track). The CPR minimum detectable signal is approximately −30 dBZ. The standard product, supplied as 2B-GEOPROF (Mace, 2007), is the radar reflectivity with a resolution of 240 m in the vertical. CloudSat overflew France at 12:55 UTC and MHS observed the scene approximately 20 min later. This represents an interesting opportunity to analyze the responses of both active and passive instruments under snowfall conditions.

AMTD
7, 7175–7206, 2014

3 Radiative transfer (RT) simulations

3.1 Simulating passive observations with ARTS

Radiative transfer (RT) simulations were performed with ARTS (Eriksson et al., 2011). ARTS is a freely available, well documented, open source software package that is well validated (Melsheimer et al., 2005; Buehler et al., 2006; Saunders et al., 2007). ARTS handles scattering with a full and efficient account of polarization effects. It provides different methods to solve the radiative transfer equation and the reverse Monte Carlo method (Davis et al., 2007) is used in this study.

The RT simulations take full account of the 3-D description of the atmospheric state modeled by Meso-NH. In order to accurately simulate satellite observations of this real scene, a correct description of the surface properties is important, especially for microwave frequency channels away from the water vapour absorption line at 183.3 ± 3 GHz. For this reason, the Tool to Estimate Land Surface Emissivities at Microwave Frequencies (TELSEM) (Aires et al., 2011) is used over land. TELSEM provides the emissivity (V and H components) for any location, any month, and any incidence angle. It is based on the analysis of the frequency, angular, and polarization dependence and it is anchored to the emissivities calculated from SSM/I observations. Similarly, the Fast Microwave Emissivity Model (FASTEM) (Liu et al., 2011) is used for ocean emissivities. FASTEM calculates sea surface emissivities from wind, sea surface temperature, and viewing angle.

3.2 The cloud radar simulator incorporated to ARTS

The equivalent radar reflectivity factor (Z_e) is the main quantitive parameter measured by radar instruments. In the absence of attenuation, the equivalent radar reflectivity factor Z_e is given by integrating the backscatter cross sections of the individual particles

AMTD
7, 7175–7206, 2014

over their size distribution:

$$Z_e = \frac{\lambda^4}{\pi^5 |K_w|^2} \int_0^\infty \sigma_b(D) n(D) \mathrm{d}D, \quad (6)$$

w here λ is the radar wavelength, $|K_w|^2$ is the reference dielectric factor (a value of 0.75 is generally used for CloudSat), σ_b is the backscatter cross section and $n(D)$ is the particle size distribution.

Recently, a module has been added to ARTS that allows the simulation of cloud radar observations. Since Eq. (6) is calculated using the single scattering properties in the same format as applied for passive observations, this module ensures a basic consistency in the microphysics assumptions independent of the technique simulated whether active or passive. Note that the module considers the two-way attenuation by gases and hydrometeors, and that multiple scattering is ignored. The single scattering assumption is a frequently accepted simplification for precipitation and cloud radar observations, although at high microwave frequencies Battaglia et al. (2008) showed that multiple scattering can significantly enhance the reflectivity profiles as observed at 94 GHz with CloudSat. For a more detailed description of this ARTS radar module, refer to the ARTS Development Version User Guide.

3.3 The hydrometeor scattering properties

The microphysical properties of the five hydrometeor categories inherent to Meso-NH, i.e., cloud, rain, ice, snow and graupel, are externally incorporated to ARTS via their particle size distribution and single scattering properties. The scattering properties of hydrometeors are related to their composition and density (and related dielectric properties), their size, their shape, and their orientation. Our analysis focuses on the evaluation of the impact and validity of different microphysical parameters in radiative transfer simulations by comparing them with the available passive and active observations.

AMTD
7, 7175–7206, 2014

a. *Density and shape:* The shape of hydrometeors is not explicitly determined by Meso-NH because they are not needed in the microphysical scheme, consequently the volume and density of particles are free parameters. However, these are crucial parameters in radiative transfer simulations as they affect the scattering properties of particles. As introduced in Sect. 2.1, the mass of each hydrometer category in Meso-NH is derived from the mass-size relation (of the type $m = aD^b$). For liquid clouds and rain, the particles are assumed to be spheres with m proportional to D^3. Although the shapes of graupel and small ice crystals are not defined strictly as spheres by Meso-NH ($b = 2.8$ and $b = 2.5$, respectively), they are approximated as such in the radiative transfer simulations of this study. Graupel are rimed particles, for which is is reasonable to assume a spherical shape. Small pure ice crystals can be approximated by spheres for microwave radiative transfer calculation as their scattering is very limited. However, snow particles are not spheres, with mass m proportional to $D^{1.9}$. A common approach in both active and passive simulations is not to describe the precise individual particle shapes, but to determine the overall shape of the particles as determined by the aspect ratio (Dungey and Bohren, 1993; Matrosov et al., 2005; Hogan et al., 2012). From multiple aircraft observations, A. J. Heymsfield (personal communication, 2013) confirms the importance of the bulk shape of particles as characterized by its aspect ratio, neglecting the microwave passive simulation of individual complicated particle shapes. Aspect ratios (longest/shortest axis of ellipse) of the order of 1.6 are investigated, as suggested in Korolev and Isaac (2003); Hanesch (2009); Matrosov et al. (2005) and Heymsfield (personal communication). In terms of density, the particle density for ice crystals is that of pure ice (0.941) and for snow and graupel, it is derived from the Meso-NH mass-size relationship.

b. *Dielectric properties:* For pure water, the dielectric properties in the microwave region are computed with limited uncertainties using Liebe et al. (1991), for instance. Similarly for pure ice, the Mätzler (2006) model is commonly adopted. For other frozen species, however, density is a key parameter in the calculation of

AMTD
7, 7175–7206, 2014

the dielectric properties. Snow and graupel can be considered as heterogeneous media, made of ice and air (dry snow and graupel) and possibly ice, air and water (wet snow). The dielectric properties can then be deduced from a number of mixing formulas. The most common, and the one used in this study, is the Maxwell Garnett formula that gives the effective dielectric constant of a mixture as a function of the dielectric constants of the host material and inclusions. For dry snow and graupel, the host is air and the inclusion is ice. For wet snow, the Maxwell Garnett formula is applied twice, once to calculate dry snow and a second time to mix dry snow and water.

c. *Single scattering properties:* The single scattering properties are calculated with the T-matrix code developed by Mishchenko (2000), which allows the treatment of spherical and non-spherical particles, as well as randomly and horizontally oriented particles. Another approach is to calculate the single scattering properties of complex shapes with the discrete-dipole approximation (DDA) (Purcell and Pennypacker, 1973). The DDA method can be used for arbitrary sized, shaped and oriented particles. Despite complicated non-spherical particles having more realistic shapes, their generation depends on idealized models that do not fully capture the large variability observed in nature. In the calculations here, the frozen particles are described by spheroids and their scattering properties are calculated from their bulk properties, i.e., dielectric properties, size and aspect ratio. This allows the use of the efficient T-matrix method. Since the spherical approximation is not always adequate for complicated aggregates (e.g. Kim, 2006; Meirold-Mautner et al., 2007; Kulie et al., 2010; Nowell et al., 2013), we also explore an approach formulated by Liu (2004) where the single scattering properties of aggregates are parameterized based on DDA modeling. Liu (2004) notes that sector-like and dendrite snowflakes have scattering and absorption properties between those of a solid ice equal-mass sphere of diameter D_0 and an ice-air mixed sphere with a diameter equal to the maximum dimension of the particle D_{max}. The dielectric properties of snow are then described by the Maxwell Garnett mixing

AMTD
7, 7175–7206, 2014

formula and the diameter of the ice equal-mass sphere is described by a softness parameter SP = $(D - D_0)/(D_{max} - D_0)$. The frequency dependent softness parameter (SP) gives the diameter of the best-fit equal-mass sphere, i.e., a frequency dependent effective density and a modified diameter is used to calculate the single scattering properties with the T-matrix. This approach has already shown a high efficiency in reproducing real observations (e.g. Meirold-Mautner et al., 2007) and it is tested here.

4 Comparison of the simulations with coincident observations

4.1 The observed and simulated scene

A close examination of MHS observations from the scene of interest (top panels of Fig. 2) and the Meso-NH outputs in Fig. 1 (and the hourly Meso-NH outputs not shown here) reveals that the cloud system modeled by Meso-NH is slightly time lagged with respect to the observations. The global structure of the cloudy scene, however, is fairly well modeled by Meso-NH in agreement with its location in the observations. With this in mind, the objective of the radiative transfer simulations is to successfully reproduce the brightness temperature depressions related to the frozen phase of the cloud. It is not to simulate the detailed spatial structure of the observations: differencies in time between the simulations and the observations (although small), added to the uncertainties in the detailed spatial structure of the front with Meso-NH would make this task unrealistic.

The first step in the radiative transfer simulations is to stay as consistent as possible with Meso-NH. In order to do this, the microphysical description of hydrometeors from Meso-NH is first used. The mass-size relationships and the particle size distributions described in Sect. 2.1 are adopted for the 5 species provided by Meso-NH (rain, cloud, ice, snow and graupel) and all hydrometeors are considered spherical. The resultant brightness temperatures from these microphysical assumptions are shown in Fig. 2

AMTD
7, 7175–7206, 2014

(bottom) as compared with the corresponding MHS observations (top). With these hypotheses, the scattering signal appears significantly less intense in the simulations, failing to reproduce the observed signal.

Figure 3 shows the distribution of the observed and simulated pixels presented in Fig. 2. Note that only pixels over land and flagged as cloudy according to a Meso-NH cut-off flag (0.05 kg m^{-2}) are included in the distributions. The statistical distributions show that for 89 and 157 GHz, observations are mostly sensitive to the snow mass column and the distribution of simulated brightness temperatures is shifted towards higher brightness temperatures (i.e., failing to reproduce the intense scattering that translates into the observed brightness temperature depressions).

The radiative transfer simulations presented so far in Figs. 2 and 3 fail to reproduce the observed scattering signatures because either (1) the amount of frozen particles produced by Meso-NH simulations is underestimated, or (2) there is a misrepresentation of the scattering properties of the frozen phase, more specifically of snow species, in the RT simulations in terms of dielectric properties, effective size, and shape.

To test these two possibilities, the availability of coincident CloudSat observations can be exploited. CloudSat observations allow comparing its different retrieved ice water path (IWP) with those modeled by Meso-NH for the CloudSat footprint, as shown in Fig. 4. In order to carry out this comparison, the three frozen species from Meso-NH are summed (ice, graupel and snow) along the CloudSat footprint. The RO-IWP product is one of CloudSat standard products and is available from the 2B-CWC-RO dataset. RO-IWP is the radar only (RO) retrieved value of IWP, obtained by assuming that the entire profile is ice, and zeroing out cases where all cloudy bins are warmer than 273 K (assumed to be liquid). The IO-RO-IWP, similarly available from the 2B-CWC-RO dataset, assumes that the entire column is ice only. DARDAR exploits lidar/radar synergy onboard the A-Train. The CPR radar can penetrate thick systems of precipitating clouds, but is mainly sensitive to large particles and does not detect small ones. The CALIOP lidar, on the other hand, is sensitive to smaller particles, but gets attenuated quickly. Therefore radar/lidar DARDAR approach (Delanoë and Hogan,

AMTD
7, 7175–7206, 2014

2008, 2010) is complementary. Despite retrieved IWP having large errors, reported by Austin et al. (2009) to be around 40 %, this qualitative comparison gives an idea of the performance of the Meso-NH, with three different retrieved products including DARDAR. Neglecting the fine structures of the CloudSat products, Meso-NH total IWP is comparable between 2.8° W and 2.9° W (mainly due to the strong presence of graupel – not shown). In the region between 2.3° W and 2.5° W, Meso-NH is comparable to the IROIWP retrieval. Overall, however, the Meso-NH outputs tend to to underestimate the total IWP when compared with CloudSat retrievals. This is not surprising given the difficulties in modeling the frozen phase, and the mentioned time lag between Meso-NH model outputs and the observations.

In an attempt to produce more scattering, the simulations in Fig. 2 are re-considered with the snow content in Meso-NH multiplied by 1.25 in each layer to match the CloudSat retrievals discussed above. This does not change the results by more than 1 K along the transect. This means that the microphysical properties require further study. The microphysical parameters describing snow particles are subject to many uncertainties, originating from the microphysical scheme of Meso-NH or on the interpretation of the Meso-NH information in terms of scattering efficiency. To answer this question we proceed to analyze the sensitivity of active and passive simulations.

4.2 Evaluation of active and passive simulations: a detailed analysis along a transect

In this section we analyse the sensitivity of the RT simulations to different microphysical assumptions of the frozen phase, focussing on the CloudSat footprint and a specific transect as described in Fig. 5. The latter transect corresponds to a specific MHS scan from close to nadir to its outermost angle north, and it is characterized by the dominance of snow in the Meso-NH outputs (Fig. 5b). The objective is to reproduce consistently the brightness temperature depressions related to the frozen phase of the cloud and the radar reflectivity with realistic microphysical properties. Again, it is not to simulate the detailed spatial structure of the observations.

AMTD
7, 7175–7206, 2014

Our objective in the radiative transfer simulations is to stay as consistent as possible with Meso-NH despite the underestimation in total IWP shown in Fig. 4. For this reason, the microphysical description of the hydrometeors from Meso-NH as used in Fig. 2 is the starting point for the radiative transfer simulations shown in Fig. 6 (shown by the black dashed line). As expected, this configuration fails to reproduce intense scattering. With these initially selected parameters, different configurations were run with different assumptions (not shown): (a) the snow size distribution was replaced by the particle size distribution of graupel, (b) perfect spheres were replaced by horizontally aligned spheroids of aspect ratio 1.6, (c) the dielectric properties of snow species were calculated with the Maxwell Garnett mixing formula but with different wetness degrees. All these microphysical assumptions failed to change significantly the simulated brightness temperatures by more than 5 K along the transect. Similarly to the conclusions drawn in Meirold-Mautner et al. (2007), snow particles that are likely to scatter radiation at 89 and 157 GHz have very low density under the Meso-NH mass-size relationship, and as a consequence they are mostly composed of air and have a very limited impact on the signal.

Changing the density of snow to a fix value of 0.1 g cm^{-3}, a value that is often used in the literature for snow, leads to a significant depression of the brightness temperatures (now shown). Similar results are obtained with horizontally aligned spheroids of aspect ratio 1.6 (solid black line). So far the density for graupel was parameterized according to Meso-NH. Setting the graupel density to a fixed value of 0.4 g cm^{-3}, a value often used in the literature for graupel, yields brightness temperatures that are much lower than those observed by MHS (not shown).

To assess the impact of the PSD on the radiometric signals for the configuration that shows good consistency with the simulations and the physical sense (snow horizontally aligned spheroids with a fixed density of 0.1 g cm^{-3} and graupel species as parameterized with Meso-NH) the Meso-NH snow PSD was replaced by Meso-NH PSD of graupel for spherical particles with fixed density (black dotted line). The particle

AMTD
7, 7175–7206, 2014

size distribution of graupel assumes fewer larger particles, and more abundant smaller particles. This causes large brightness temperature depressions.

Finally, the approach suggested by Liu (2004) to approximate the single scattering properties of snow species calculated with the DDA method is analyzed. For 85 and 150 GHz, a softness parameter SP = $(D - D_0)/(D_{max} - D_0)$ was derived by Liu (2004) yielding the diameter of the best-fit equal mass sphere. The frequency dependent softness parameter SP gives the diameter of the best-fit equal-mass sphere, i.e., a frequency dependent effective density and a modified diameter is used to calculate the single scattering properties with the T-matrix. As shown in Fig. 6, the results are very encouraging in accordance with the observed TBs (red dotted line). Analyzing the sensitivity of these assumptions to the snow content by multiplying it by 1.25 each atmospheric layer shows that the improvement is not significant in terms of brightness temperatures (blue dotted line).

The CloudSat response is then simulated based on the analysis conducted for the passive simulations. Figure 7 (left column) presents the active simulations using the coincident Meso-NH species contents as shown in Fig. 4. The first step is to simulate the active response assuming the initial microphysical properties from the Meso-NH scheme, which proved to underestimate the scattering efficiency for passive radiative transfer simulations. The results are shown in Fig. 7a for perfect spheres. The overall 3-D structure of the observed reflectivity, given the scales of the Meso-NH output, are captured reasonably well (Meso-NH has 5 km resolution, while the nadir CloudSat footprint has 1.4 km resolution). It is evident, however, that such microphysical assumptions also underestimate the backscattering properties, for the same reason as with passive simulations. Replacing the Meso-NH parameterization of mass by a fixed density of 0.1 g cm^{-3} as done for passive simulations only yields a slight improvement. Figure 7b shows fixed density horizontally aligned spheroids of aspect ratio 1.6. Only a slight improvement is observed with higher reflectivities where the Meso-NH total ice content is higher and closer to retrieved products (mainly around 2.4° W and east of 3° W – see Fig. 4). The Liu (2004) approximation is also tested for the active response for perfect

AMTD
7, 7175–7206, 2014

spheres (not shown) and in Fig. 7c for horizontally aligned spheroids of aspect ration 1.6. The reflectivity is still systematically underestimated, regardless of the hypothesis. Based on conclusions drawn from Fig. 4 and the analysis of passive simulations, Fig. 7 (right column) presents the same active simulations above, but multiplying the snow quantities systematically by 1.25 to account for the underestimation of the Meso-NH IWP. The comparisons with the observations are not better in the case of the Meso-NH hypothesis, but they are significantly improved with the Liu (2004) approximation. As previously discussed, this same configuration was shown to work well with the passive simulations. This is very encouraging, and shows that we can reasonably simulate both passive and active observations, with careful and consistent assumptions about the parameters that determine the scattering properties. Figure 8 shows the simulations for those MHS channels most sensitive to the frozen phase using these last assumptions (the Liu, 2004 approximation and multiplying the snow quantities systematically by 1.25), as compared to the previously introduced observations and simulations. The new simulations enhance scattering.

5 Conclusions

Microwave passive and active radiative transfer simulations are presented for a specific snowfall mid-latitude scene, using outputs from the Meso-NH mesoscale cloud model and compared to the corresponding microwave observations available from MHS and CloudSat. The sensitivity of radiative transfer simulations to the microphysical characteristics of the frozen particles (size, density, dielectric properties) is the focus of this study.

The radiative transfer simulations were performed by coupling ARTS and its recently incorporated active simulator module, to the mesoscale cloud model Meso-NH. Performing a comparison of simulations and observations over a large range of frequencies and exploiting the passive/active synergy is a challenging but useful task because it imposes strong constraints on the assumptions made to simulate the observations.

AMTD
7, 7175–7206, 2014

Disregarding the detailed spatial structures which would make this task unrealistic, an overall agreement is obtained between the simulated and the observed brightness temperatures (passive) and radar reflectivities (active). The large scale dynamical structure of the cloud system is reasonably captured by Meso-NH, however, comparisons between the radiative transfer simulations and the available observations show a misrepresentations in the areas of strong scattering. From our sensitivity analysis, the failure to reproduce the observed strong scattering signals arises from the interpretation of Meso-NH microphysical parameterisations of snow particles in the radiative transfer simulations.

Nonetheless, both passive and active radiative transfer simulations showed very encouraging results, as we can reasonably simulate available observations from consistent assumptions on the parameters that determine the scattering properties, specially with the Liu (2004) approximation. The Liu (2004) approximation provides a frequency dependent effective density for snow particles that results in more realistic scattering properties. Hence, it is important to conclude that the microphysical assumptions in the Meso-NH scheme are realistic, provided that they are well interpreted in the scattering calculation. This is an important step towards building a robust dataset of simulated measurements to train a statistically base retrieval scheme.

Acknowledgements. The ARTS community is appreciated for providing, developing and maintaining such an open source software.

References

Aires, F., Prigent, C., Bernardo, F., Jiménez, C., Saunders, R., and Brunel, P.: A tool to estimate land-surface emissivities at microwave frequencies (TELSEM) for use in numerical weather prediction, Q. J. Roy. Meteor. Soc., 137, 690–699, 2011. 7183

Austin, R. T., Heymsfield, A. J., and Stephens, G. L.: Retrieval of ice cloud microphysical parameters using the CloudSat millimeter-wave radar and temperature, J. Geophys. Res.-Atmos., 114, D00A23, doi:10.1029/2008JD010049, 2009. 7189

AMTD
7, 7175–7206, 2014

Battaglia, A., Haynes, J., L'Ecuyer, T., and Simmer, C.: Identifying multiple-scattering-affected profiles in CloudSat observations over the oceans, J. Geophys. Res.-Atmos., 113, D00A17, doi:10.1029/2008JD009960, 2008. 7184

Bennartz, R. and Bauer, P.: Sensitivity of microwave radiances at 85–183 GHz to precipitating ice particles, Radio Sci., 38, 8075, doi:10.1029/2002RS002626, 2003. 7178

Bonsignori, R.: The Microwave Humidity Sounder (MHS): in-orbit performance assessment, in: Remote Sensing, International Society for Optics and Photonics, 67440A–67440A, Florence, Italy, 2007. 7182

Buehler, S. A., Courcoux, N., and John, V. O.: Radiative transfer calculations for a passive microwave satellite sensor: comparing a fast model and a line-by-line model, J. Geophys. Res., 111, D20304, doi:10.1029/2005JD006552, 2006. 7183

Chaboureau, J.-P., Cammas, J.-P., Mascart, P., Pinty, J.-P., Claud, C., Roca, R., and Morcrette, J.-J.: Evaluation of a cloud system life-cycle simulated by the Meso-NH model during FASTEX using METEOSAT radiances and TOVS-3I cloud retrievals, Q. J. Roy. Meteor. Soc., 126, 1735–1750, 2000. 7179

Chaboureau, J.-P., Söhne, N., Pinty, J.-P., Meirold-Mautner, I., Defer, E., Prigent, C., Pardo, J. R., Mech, M., and Crewell, S.: A midlatitude precipitating cloud database validated with satellite observations, J. Appl. Meteorol. Clim., 47, 1337–1353, doi:10.1175/2007JAMC1731.1, 2008. 7179

Davis, C. P., Evans, K. F., Buehler, S. A., Wu, D. L., and Pumphrey, H. C.: 3-D polarised simulations of space-borne passive mm/sub-mm midlatitude cirrus observations: a case study, Atmos. Chem. Phys., 7, 4149–4158, doi:10.5194/acp-7-4149-2007, 2007. 7183

Delanoë, J. and Hogan, R. J.: A variational scheme for retrieving ice cloud properties from combined radar, lidar, and infrared radiometer, J. Geophys. Res.-Atmos., 113, D07204, doi:10.1029/2007JD009000, 2008. 7188

Delanoë, J. and Hogan, R. J.: Combined CloudSat-CALIPSO-MODIS retrievals of the properties of ice clouds, J. Geophys. Res.-Atmos., 115, D00H29, doi:10.1029/2009JD0123462010, 2010. 7189

Dungey, C. and Bohren, C. F.: Backscattering by nonspherical hydrometeors as calculated by the coupled-dipole method – An application in radar meteorology, J. Atmos. Ocean. Tech., 10, 526–532, 1993. 7185

AMTD
7, 7175–7206, 2014

Eliasson, S., Buehler, S. A., Milz, M., Eriksson, P., and John, V. O.: Assessing observed and modelled spatial distributions of ice water path using satellite data, Atmos. Chem. Phys., 11, 375–391, doi:10.5194/acp-11-375-2011, 2011. 7178
Eriksson, P., Buehler, S., Davis, C., Emde, C., and Lemke, O.: ARTS, the atmospheric radiative transfer simulator, version 2, J. Quant. Spectrosc. Ra., 112, 1551–1558, 2011. 7183
Hanesch, M.: Fall velocity and shape of snowflakes, Ph. D. thesis, Swiss Federal Institute of Technology, 2009. 7185
Hogan, R. J., Tian, L., Brown, P. R. A., Westbrook, C. D., Heymsfield, A. J., and Eastment, J. D.: Radar scattering from ice aggregates using the horizontally aligned oblate spheroid approximation, J. Appl. Meteorol. Clim., 51, 655–671, 2012. 7185
Johnson, B. T., Petty, G. W., and Skofronick-Jackson, G.: Microwave properties of ice-phase hydrometeors for radar and radiometers: sensitivity to model assumptions, J. Appl. Meteorol. Clim., 51, 2152–2171, 2012. 7178
Katsumata, M., Uyeda, H., Iwanami, K., and Liu, G.: The response of 36- and 89-GHz microwave channels to convective snow clouds over ocean: observation and modeling, J. Appl. Meteorol., 39, 2322–2335, 2000. 7178
Kim, M.-J.: Single scattering parameters of randomly oriented snow particles at microwave frequencies, J. Geophys. Res.-Atmos., 111, D14201, doi:10.1029/2005JD006892, 2006. 7186
Korolev, A. and Isaac, G.: Roundness and aspect ratio of particles in ice clouds, J. Atmos. Sci., 60, 1795–1808, 2003. 7185
Kulie, M. S., Bennartz, R., Greenwald, T. J., Chen, Y., and Weng, F.: Uncertainties in microwave properties of frozen precipitation: implications for remote sensing and data assimilation, J. Atmos. Sci., 67, 3471–3487, 2010. 7186
Lafore, J. P., Stein, J., Asencio, N., Bougeault, P., Ducrocq, V., Duron, J., Fischer, C., Héreil, P., Mascart, P., Masson, V., Pinty, J. P., Redelsperger, J. L., Richard, E., and Vilà-Guerau de Arellano, J.: The Meso-NH Atmospheric Simulation System. Part I: adiabatic formulation and control simulations, Ann. Geophys., 16, 90–109, doi:10.1007/s00585-997-0090-6, 1998. 7179
Liebe, H. J., Hufford, G. A., and Manabe, T.: A model for the complex permittivity of water at frequencies below 1 THz, Int. J. Infrared Milli., 12, 659–675, 1991. 7185
Liu, G.: Approximation of single scattering properties of ice and snow particles for high microwave frequencies, J. Atmos. Sci., 61, 2441–2456, 2004. 7186, 7191, 7192, 7193, 7206
Liu, Q., Weng, F., and English, S.: An improved fast microwave water emissivity model, IEEE T. Geosci. Remote, 49, 1238–1250, 2011. 7183

AMTD
7, 7175–7206, 2014

Mace, G.: Level 2 GEOPROF product process description and interface control document algorithm version 5.3, NASA Jet Propulsion Laboratory, 2007. 7182
Matrosov, S. Y., Heymsfield, A. J., and Wang, Z.: Dual-frequency radar ratio of nonspherical atmospheric hydrometeors, Geophys. Res. Lett., 32, L13816, doi:10.1029/2005GL023210, 2005. 7185
Mätzler, C.: Thermal Microwave Radiation: Applications for Remote Sensing, vol. 52, Iet, 2006. 7185
Meirold-Mautner, I., Prigent, C., Defer, E., Pardo, J. R., Chaboureau, J.-P., Pinty, J.-P., Mech, M., and Crewell, S.: Radiative transfer simulations using mesoscale cloud model outputs: comparisons with passive microwave and infrared satellite observations for midlatitudes, J. Atmos. Sci., 64, 1550–1568, 2007. 7179, 7186, 7187, 7190
Melsheimer, C., Verdes, C., Buehler, S. A., Emde, C., Eriksson, P., Feist, D. G., Ichizawa, S., John, V. O., Kasai, Y., Kopp, G., Koulev, N., Kuhn, T., Lemke, O., Ochiai, S., Schreier, F., Sreerekha, T. R., Suzuki, M., Takahashi, C., Tsujimaru, S., and Urban, J.: Intercomparison of general purpose clear sky atmospheric radiative transfer models for the millimeter/submillimeter spectral range, Radio Sci., 40, RS1007, doi:10.1029/2004RS003110, 2005. 7183
Mishchenko, M. I.: Calculation of the amplitude matrix for a nonspherical particle in a fixed orientation, Appl. Optics, 39, 1026–1031, 2000. 7186
Noh, Y.-J., Liu, G., Seo, E.-K., Wang, J. R., and Aonashi, K.: Development of a snowfall retrieval algorithm at high microwave frequencies, J. Geophys. Res.-Atmos., 111, D22216, doi:10.1029/2005JD006826, 2006. 7177
Nowell, H., Liu, G., and Honeyager, R.: Modeling the microwave single-scattering properties of aggregate snowflakes, J. Geophys. Res.-Atmos., 118, 7873–7885, 2013. 7186
Pinty, J. and Jabouille, P.: A mixed-phase cloud parameterization for use in a mesoscale nonhydrostatic model: simulations of a squall line and of orographic precipitations, in: Conf. on Cloud Physics, 217–220, 1998. 7179
Purcell, E. M. and Pennypacker, C. R.: Scattering and absorption of light by nonspherical dielectric grains, Astrophys. J., 186, 705–714, 1973. 7186
Saunders, R., Rayer, P., Brunel, P., von Engeln, A., Bormann, N., Strow, L., Hannon, S., Heilliette, S., Liu, X., Miskolczi, F., Han, Y., Masiello, G., Moncet, J.-L., Uymin, G., Sherlock, V., and Turner, D. S.: A comparison of radiative transfer models for simulating Atmospheric Infrared

AMTD
7, 7175–7206, 2014

Sounder (AIRS) radiances, J. Geophys. Res., 112, D01S90, doi:10.1029/2006JD007088, 2007. 7183

Skofronick-Jackson, G. and Johnson, B.: Thresholds of detection for falling snow from satellite-borne active and passive sensors, in: Geoscience and Remote Sensing Symposium (IGARSS), 2011 IEEE International, 2637–2640, 2011. 7178

Stephens, G. L., Vane, D. G., Boain, R. J., Mace, G. G., Sassen, K., Wang, Z., Illingworth, A. J., O'Connor, E. J., Rossow, W. B., Durden, S. L., Miller, S. D., Austin, R. T., Benedetti, A., Mitrescu, C., and the CloudSat Science Team: The cloudsat mission and the A-train, B. Am. Meteorol. Soc., 83, 1771–1790, 2002. 7182

Waliser, D. E., Li, J.-L. F., Woods, C. P., Austin, R. T., Bacmeister, J., Chern, J., Del Genio, A., Jiang, J. H., Kuang, Z., Meng, H., Minnis, P., Platnick, S., Rossow, W. B., Stephens, G. L., Sun-Mack, S., Tao, W.-K., Tompkins, A. M., Vane, D. G., Walker, C., and Wu, D.: Cloud ice: a climate model challenge with signs and expectations of progress, J. Geophys. Res.-Atmos., 114, D00A21, doi:10.1029/2008JD010015, 2009. 7178

Wiedner, M., Prigent, C., Pardo, J. R., Nuissier, O., Chaboureau, J.-P., Pinty, J.-P., and Mascart, P.: Modeling of passive microwave responses in convective situations using output from mesoscale models: comparison with TRMM/TMI satellite observations, J. Geophys. Res.-Atmos., 109, D06214, doi:10.1029/2003JD004280, 2004. 7179

AMTD
7, 7175–7206, 2014

Table 1. Parameters of the Meso-NH microphysical scheme described by Eqs. (1) through (5) (given in mks units).

Category	α	ν	a	b	c	d	C	x
q_c (cloud)	3	3	524	3	3.2×10^7	2		
q_i (ice)	3	3	0.82	2.5	800	1		
q_s (snow)	1	1	0.02	1.9	5.1	0.27	5	1
q_g (graupel)	1	1	19.6	2.8	124	0.66	5×10^5	−0.5
q_r (rain)	1	1	524	3	824	0.8	10^7	−1

AMTD
7, 7175–7206, 2014

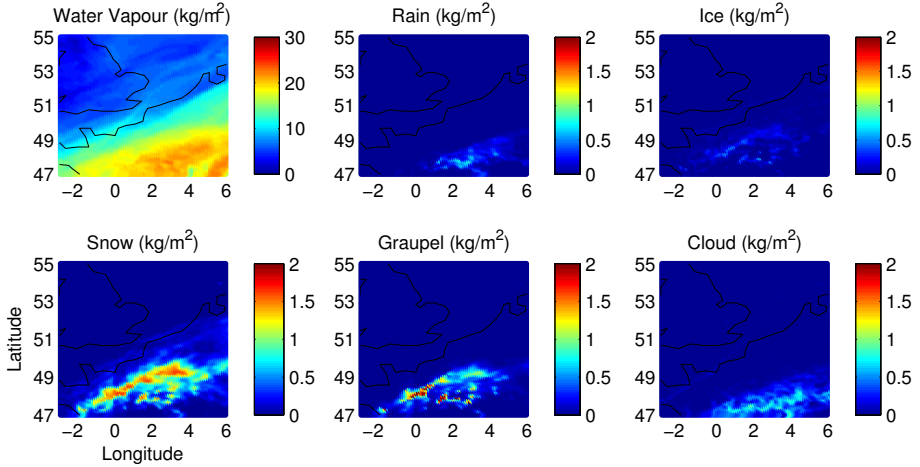

Figure 1. The Meso-NH fields at 13:00 UTC of the heavy snowfall scene over France on 8 December 2010. Coincident observations from MHS and CloudSat are available.

AMTD
7, 7175–7206, 2014

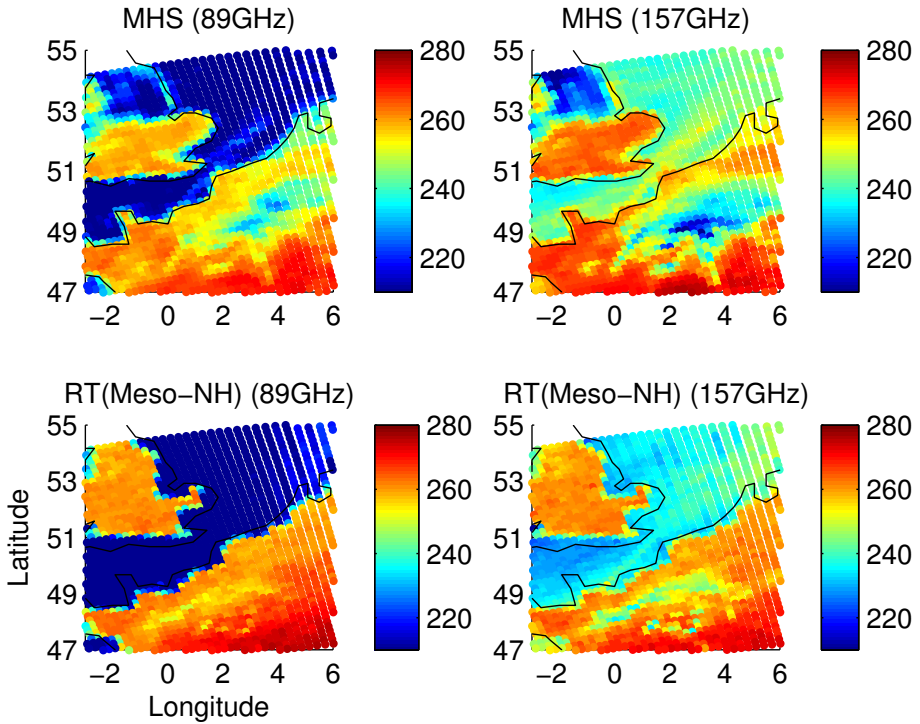

Figure 2. MHS observations at 89 GHz and 157 GHz (top panel), as compared with the corresponding simulated brightness temperatures with the microphysical scheme intrinsic to Meso-NH (bottom panel).

AMTD
7, 7175–7206, 2014

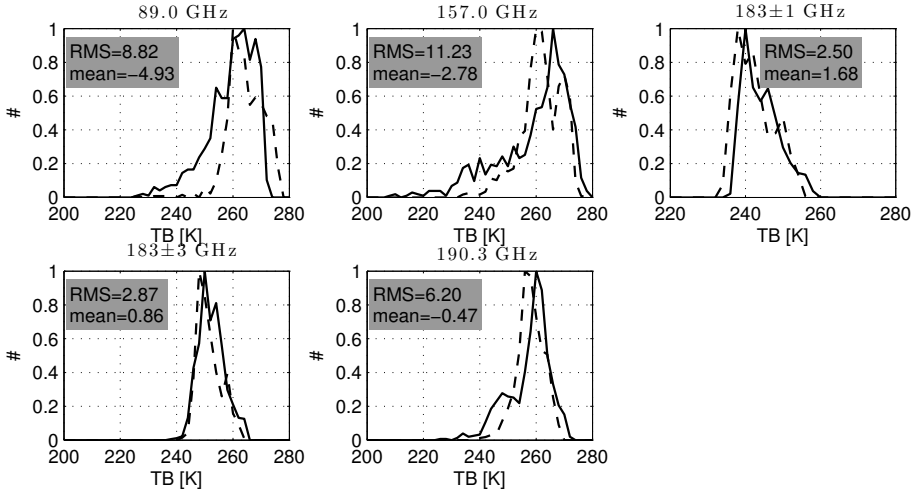

Figure 3. Histograms of the observed (solid line) and simulated (dashed line) MHS brightness temperatures with the Meso-NH microphysical scheme. The data used to calculate these distributions correspond to cloudy pixels (as determined my Meso-NH) over land as presented in Fig. 2. The RMS and bias of the difference between the two are indicated for each frequency.

AMTD
7, 7175–7206, 2014

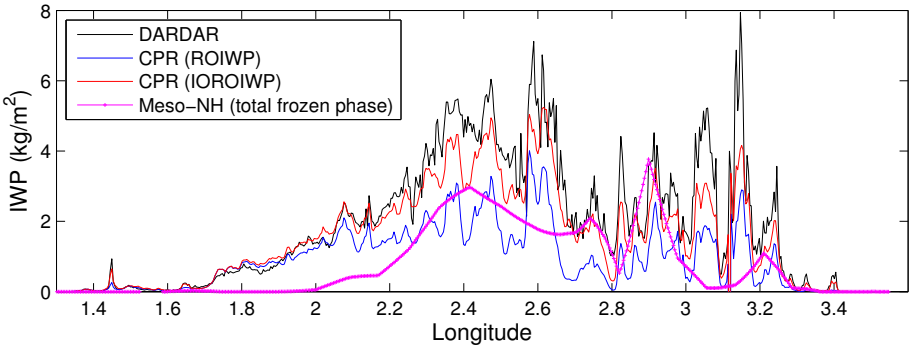

Figure 4. CloudSat CPR ice mass content as retrieved by DARDAR, CWC-RO and CWC-IO-RO. The total frozen mass contents (graupel + ice + snow) modeled by Meso-NH are shown for reference.

AMTD
7, 7175–7206, 2014

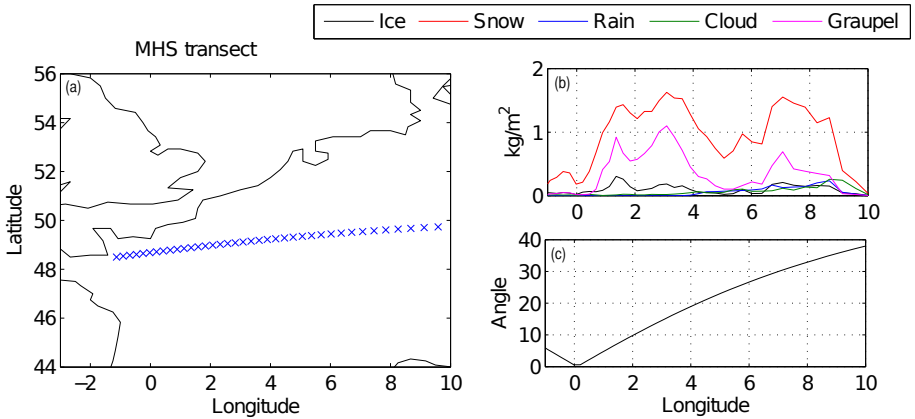

Figure 5. Selected transect of the case study: **(a)** the location of the transect; **(b)** the integrated content of the different Meso-NH hydrometeors along this transect; and **(c)** the incidence angle of the MHS observations along the transect.

AMTD
7, 7175–7206, 2014

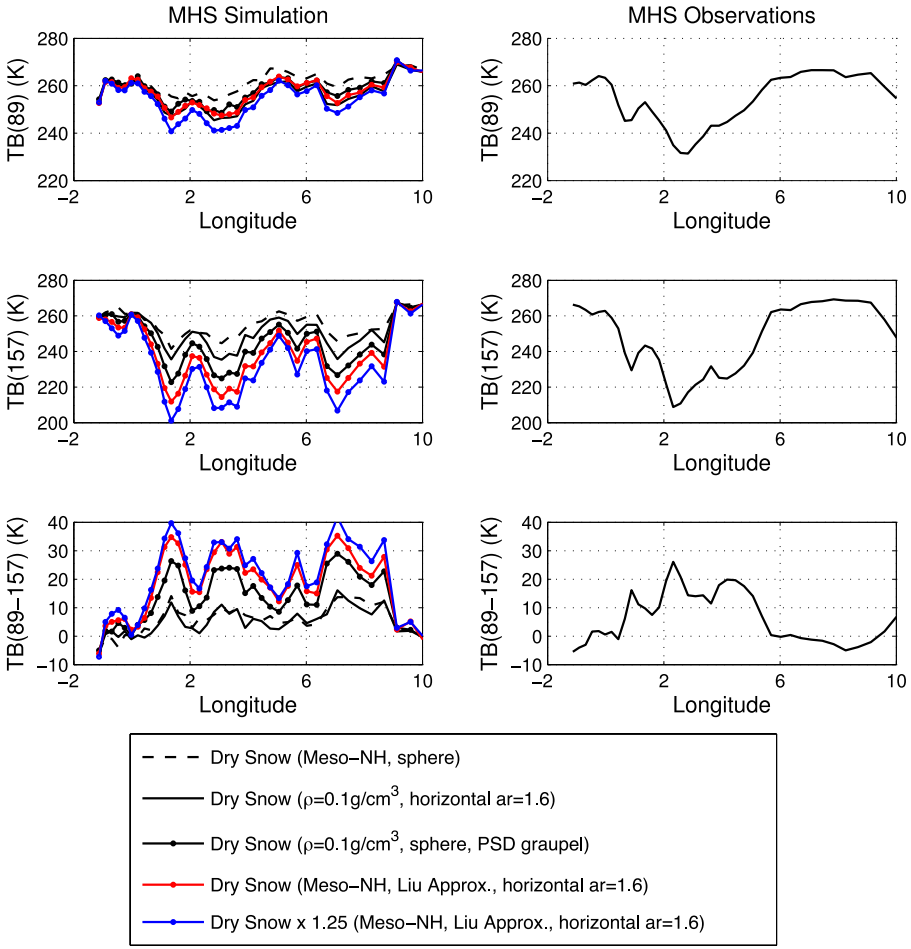

Figure 6. The observed (right) and simulated (left) brightness temperature measurements from the MHS window channels along the chosen transect presented in Fig. 5.

AMTD
7, 7175–7206, 2014

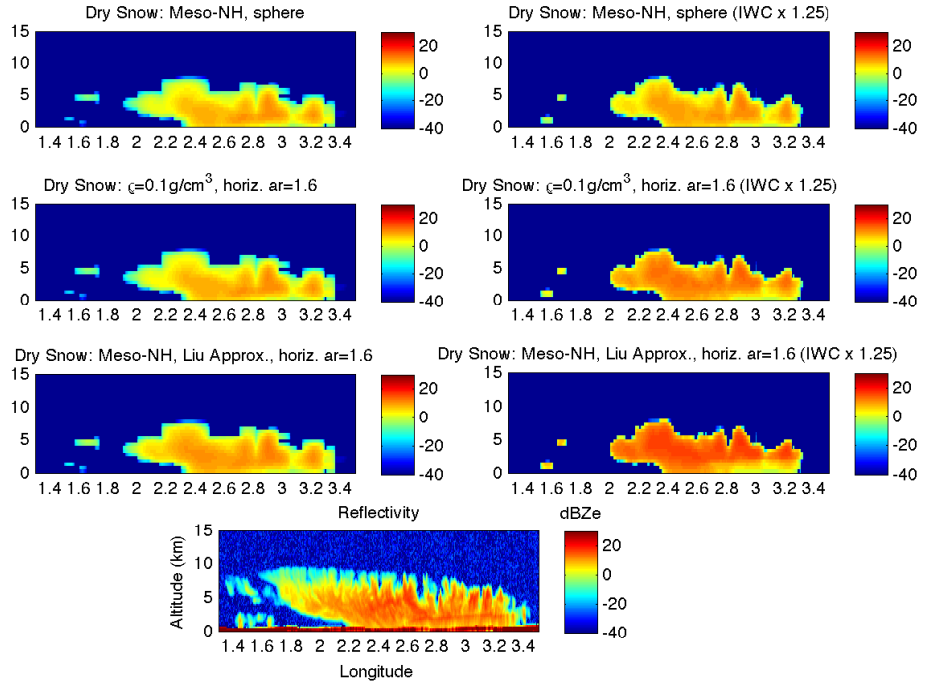

Figure 7. The simulated CPR (94 GHz) radar reflectivity. See individual figure titles for more information. CloudSat CPR radar reflectivity (94 GHz) is also shown.

AMTD
7, 7175–7206, 2014

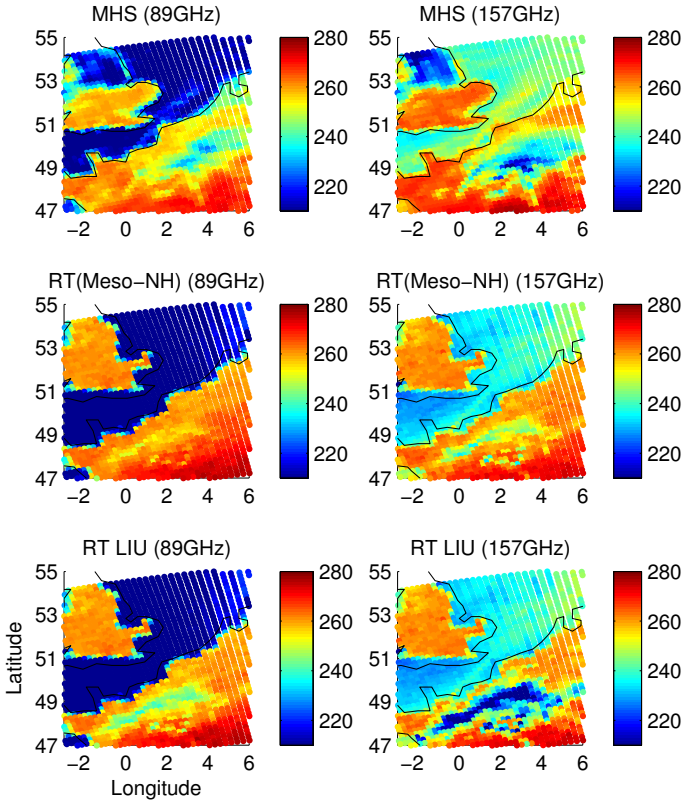

Figure 8. MHS observations at 89 and 157 GHz (top panels), as compared to its radiative transfer simulations using the first assumptions intrinsic to the microphysical scheme of Meso-NH (middle panels), and the Meso-NH intrinsic scheme together with the Liu (2004) approximation and multiplying the snow quantities systematically by 1.25 (bottom panels).

AMTD
7, 7175–7206, 2014